Kinetic characterization and modeling of a microalgae consortium isolated from landfill leachate under a high CO_2 concentration in a bubble column photobioreactor

Luis Fernando Saldarriaga [a,b], Fernando Almenglo [a], Martín Ramírez [a,*], Domingo Cantero [a]

[a] Departamento de Ingeniería Química y Tecnología de Alimentos, Instituto de Investigación Vitivinícola y Agroalimentaria, Universidad de Cadiz, Puerto Real 11510, Spain
[b] Departamento de Química, Universidad del Atlántico, Km 7, Vía Puerto Colombia, Colombia

ARTICLE INFO

ABSTRACT

Background: The determination of kinetic parameters and the development of mathematical models are of great interest to predict the growth of microalgae, the consumption of substrate and the design of photobioreactors focused on CO_2 capture. However, most of the models in the literature have been developed for CO_2 concentrations below 10%.

Results: A nonaxenic microalgal consortium was isolated from landfill leachate in order to study its kinetic behavior using a dynamic model. The model considered the CO_2 mass transfer from the gas phase to the liquid phase and the effect of light intensity, assimilated nitrogen concentration, ammonium concentration and nitrate concentration. The proposed mathematical model was adjusted with 13 kinetic parameters and validated with a good fit obtained between experimental and simulated data.

Conclusions: Good results were obtained, demonstrating the robustness of the proposed model. The assumption in the model of DIC inhibition in the ammonium and nitrate uptakes was correct, so this aspect should be considered when evaluating the kinetics with microalgae with high inlet CO_2 concentrations.

How to cite: Saldarriaga L F, Almenglo F, Ramírez M, et al. Kinetic characterization and modeling of a microalgae consortium isolated from landfill leachate under a high CO2 concentration in a bubble column photobioreactor. Electron J Biotechnol 2020;44. https://doi.org/10.1016/j.ejbt.2020.01.006.

Nomenclature

Symbol	Definition	Units
$C_{L,CO2}$	Carbon dioxide concentration in liquid phase	[mg CO_2 L^{-1}]
$C^*_{L,CO2}$	Carbon dioxide concentration in liquid phase in equilibrium with gas phase	[mg CO_2 L^{-1}]
$C_{G,CO2}$	Carbon dioxide concentration in gas phase	[mg CO_2 L^{-1}]
$C_{G,CO2,IN}$	Inlet carbon dioxide concentration in gas phase	[mg CO_2 L^{-1}]
$C_{L,NO3}$	Nitrate concentration in liquid phase	[mg N-NO_3^- L^{-1}]
$C_{L,NH4}$	Ammonium concentration in liquid phase	[mg N-NH_4^+ L^{-1}]
$C_{DIC,X}$	Total dissolved inorganic carbon concentration	[mg CO_2 L^{-1}]
C_N	Concentration of assimilated nitrogen as amino acids	[mg N L^{-1}]
μ	Specific growth rate	[h^{-1}]
μ_{max}	Maximum specific growth rate	[h^{-1}]
$q_{max,NO3}$	Maximum specific nitrate uptake	[mg N-NO_3^- mg TSS^{-1} L^{-1}]
$q_{max,NH4}$	Maximum specific ammonium uptake	[mg N-NH_4^+ mg TSS^{-1} L^{-1}]
$q_{s,NO3}$	Specific nitrate uptake	[mg N-NO_3^- mg TSS^{-1} L^{-1}]
$q_{s,NH4}$	Specific ammonium uptake	[mg N-NH_4^+ mg TSS^{-1} L^{-1}]
$K_{S,N}$	Monod half-saturation constant for nitrogen	[mg N L^{-1}]
$K_{S,NO3}$	Monod half-saturation constant for nitrate	[mg N-NO_3^- L^{-1}]
$K_{S,NH4}$	Monod half-saturation constant for ammonium	[mg N-NH_4^+ L^{-1}]
$K_{S,I\,avg}$	Monod half-saturation constant for light intensity	[μmol m^{-2} s^{-1}]
$K_{DIC,X}$	Inhibition constant for DIC	[mg C L^{-1}]
$K_{DIC,NO3}$	Inhibition constant for DIC (nitrate uptake)	[mg C L^{-1}]
$K_{DIC,NH4}$	Inhibition constant for DIC (ammonium uptake)	[mg C L^{-1}]
K_{NH4}	Inhibition constant of ammonium	[mg N-NH_4^+ L^{-1}]
$K_{i,NH4}$	Haldane inhibition constant for ammonium	[mg N-NH_4^+ L^{-1}]
$K_{i,N}$	Haldane inhibition constant for nitrogen	[mg N L^{-1}]
I_{avg}	Light intensity average	[μmol m^{-2} s^{-1}]
$K_{La,CO2}$	Carbon dioxide mass transfer coefficient	[h^{-1}]
$K_{La,O2}$	Oxygen mass transfer coefficient	[h^{-1}]
$k_{a,1}$	Dissociation constant for bicarbonate	[mol L^{-1}]
$k_{a,2}$	Dissociation constant for carbonate	[mol L^{-1}]
H_{CO2}	Henry's constant (CO_2)	[mol m^{-3} atm^{-1}]
X	Biomass concentration	[g L^{-1}]

* Corresponding author.
 E-mail address: martin.ramirez@uca.es (M. Ramírez).
Peer review under responsibility of Pontificia Universidad Católica de Valparaíso.

$Y_{X/CO2}$	Yield coefficient of biomass per CO_2 uptake	[mg N mg TSS^{-1}]
$Y_{X/N}$	Yield coefficient of biomass per nitrogen uptake	[mg CO_2 mg TSS^{-1}]
F_G	Gas flow rate	[m^3 h^{-1}]
V_G	Volume of gas hold-up	[m^3]
V_L	Volume of medium in the photobioreactor	[m^3]
m	Dimensionless gas–liquid equilibrium constant	[-]
Y	Predicted response (Yield coefficient)	[g g^{-1}]
α_0	Intercept	[-]
α_1, α_2	Linear coefficients	[-]
α_{11}, α_{22}	Square coefficients	[-]
α_{12}	Interaction coefficient	[-]
X_1, X_2	Coded independent factors	[-]
P_b	Biomass productivity	[g TSS L^{-1} d^{-1}]
X_{max}	Maximum microalgae concentration	[g L^{-1}]
X_o	Initial microalgae concentration	[g L^{-1}]
t_m	Time required to reach X_{max}	[h]
t_o	Time required to reach X_o	[h]
PFD_{AVE}	Average photon flux density	[μmol m^{-2} s^{-1}]
PFD_{IN}	Incident photon flux density	[μmol m^{-2} s^{-1}]
PFD_0	Photon flux density in the light surface	[μmol m^{-2} s^{-1}]
α_x	Specific absorption coefficient of the biomass	[m^2 g^{-1}]
$\alpha_x(\lambda)$	Wavelength-dependent specific absorption coefficient of biomass	[m^2 g^{-1} nm^{-1}]
δ	Reactor light path	[m]
λ	wavelength	[nm]
a_a	Air absorption coefficient	[m^{-1}]
L	Length	[m]
Am	Methacrylate absorbance	[-]
OF_{NH4}	Ammonium objective function	[mg N-NH_4^+ L^{-1}]
OF_{NO3}	Nitrate objective function	[mg N-NO_3^- L^{-1}]
OF_X	Biomass objective function	[mg TSS L^{-1}]

1. Introduction

Global warming, which is caused by the gradual increase in greenhouse gases, is a world-wide problem that requires urgent solutions. In this sense, CO_2 emissions contribute approximately 65% of total greenhouse gases, with an annual estimated CO_2 release of 4.13 Gt [1]. Low-cost technologies based on microalgae are of particular interest in CO_2 capture since the photosynthetic efficiency is in the range 3–8%, compared to the value for terrestrial plants of 0.5%. Effluents with high CO_2 concentrations include flue gases (i.e., cement industry, coal plants, biomass boiler plants, etc.), biogas and alcoholic fermentation processes. For example, biogas has a methane content of 55–75% and CO_2 in the range 20–55% along with other minor gases [2].

The main concerns in relation to microalgae-based photobioreactors are the microalgal growth and the nutrient uptake. Consequently, it is necessary to optimize the operational conditions to maximize the growth and photobioreactor performance and it is also advantageous to develop a mathematical model for the system. There are models for microalgal growth kinetics that consider multiple factors, e.g. nitrogen, phosphorus, CO_2, organic carbon, light and temperature. However, most of the models in the literature have been developed for CO_2 concentrations below 10% [3–7]. Huseh et al. [3] simulated CO_2 concentrations of 5, 8, 10, 20 and 40% for carbon bio-fixation by *Thermosynechococcus* sp. CL-1 and *Nannochloropsis oculata* and they found that at 10% the growth was completely inhibited. In addition, the inhibition effect of CO_2 concentrations above 10% was described for *Chlorella* sp. [8,9]. Kasiri et al. [8] described the CO_2 effect on the growth of a *Chlorella kessleri* culture for a CO_2 concentration between 8 and 42% using a Haldane-like & Caperon–Meyer kinetic model. Lee and Zhang [9] used a Haldane-like expression to describe the growth of *Chlorella* sp. for a CO_2 concentration up to 15%. As far as we know, Dissolved Inorganic Carbon (DIC) inhibition in growth and nutrient absorption has not been described for CO_2 concentrations greater than 10%. It is therefore necessary to determine the kinetic parameters at high CO_2 concentrations above 10% in order to model, realistically, the treatment of CO_2-rich effluents.

The present study is focused on describing the inhibitory effect of the CO_2 concentration (5–30%) on the nitrogen uptake and microalgae growth. The dynamic model described herein was used in batch experiments (calibration stage) and could be applied satisfactorily in continuous experiments (validation stage) with slight mass balance modifications. The aim of the work reported here was to obtain a microalgal consortium that was able to use landfill leachate as a nitrogen source and to develop, calibrate and validate a dynamic model that was capable of predicting the biomass, ammonium and nitrate concentrations at high inlet CO_2 concentrations. The model was developed through the application of mass balances and the definition of the main processes that occur in a photobioreactor.

2. Material and methods

2.1. Microalgae culture and isolation

A microalgae consortium, nonaxenic, was isolated from landfill leachate obtained from 'Miramundo los Hardales' Landfill (Cádiz), location: 36°28′42.5″N 6°00′56.1″W. 500 mL of Combo medium [10] enriched in phosphorus (5 mM) and nitrogen (5 mM $NaNO_3$) was inoculated with leachate (5% v v^{-1}). The leachate composition from the landfill without dilution was as follows (mg L^{-1}): Chemical Oxygen Demand (COD) (9465.3), alkalinity (24,898.9), TSS (24,230.1), total phosphorus (87.1), P-PO_4^{3-} (48.8), total nitrogen (5731.4) N-NH_4^+ (4682.4), N-NO_3^- (13.3). The pH and conductivity were 8.15 and 45.7 mS cm^{-1}, respectively.

Cultivation was carried out in an Erlenmeyer flask (1 L) using CO_2 (5% in air) as the carbon source. A mixture of air and CO_2 was bubbled at a constant rate of 0.2 vvm. Each Erlenmeyer flask was illuminated with Light-Emitting Diode (LED) lamps (6500 K, 18 W, F-Bright Eco, Spain) with a photoperiod of 12:12 light:dark cycles, with an average surface irradiance of 180 μmol m^{-2} s^{-1}. The temperature was maintained at 20–25°C by an air conditioner. 30% of the culture was replaced with fresh medium every week until the growth of microalgae was observed. A nonaxenic consortium was obtained by serial dilution using an initial biomass concentration of 10^6 cells mL^{-1} [11]. Repetition of dilutions 1:10 in 10 mL tubes was done and the tube with the highest dilution that showed microalgae growth was selected. The nonaxenic culture (10 mL) was carried out in an Erlenmeyer flask (0.25 L) with combo Medium and then transferred to a 1 L culture using CO_2 (5% in air) at 1 vvm.

2.2. Experimental set-up and operational conditions in the model calibration

The microalgae consortium was grown in two bubble column photobioreactors. These were made of transparent polymethyl methacrylate (Plásticos Ferplast S.L., Spain), with an inner diameter of 9.4 cm and a height of 100 cm (working volume of 8 L). A schematic diagram of the system for a single photobioreactor is shown in Fig. 1 along with the light distribution for both reactors (Fig. 1a). A mixture of air and CO_2 was fed into the column with inlet CO_2 concentrations of 5, 10, 20 and 30% v v^{-1}. A gas flow rate of 0.1 vvm was selected based on the results obtained by Thawechai et al. [12]. Two stone air diffusers (10 μm, Slip-on inlet filter, Supelco, USA) were used for aeration. A mass flow controller (F-201 CV, Bronkhorst High-Tech B.V., The Netherlands) was used to fix the inlet CO_2 concentration and a variable area flow meter (FR2A12BVBN, Key Instruments, UK) was used to measure the air flow rate. On the top of the column the pH and Dissolved Oxygen (DO) were monitored (Multimeter M44, Crison Instruments S.A., Spain). The optimal temperature value for microalgae growth is between 15–26°C [13]. So, an intermediate temperature value of 20 ± 1°C was selected and kept constant by recirculation of 830 mL h^{-1} of the culture to a thermostatic bath (RA-8 alpha, LAUDA, Germany). The photobioreactors were illuminated with 7 LED lamps (6500 K, 18 W, F-Bright Eco, Spain) with a photoperiod of 12:12 light:dark cycles, average surface irradiance of 220 μmol m^{-2} s^{-1} (Fig. 1a). The system was
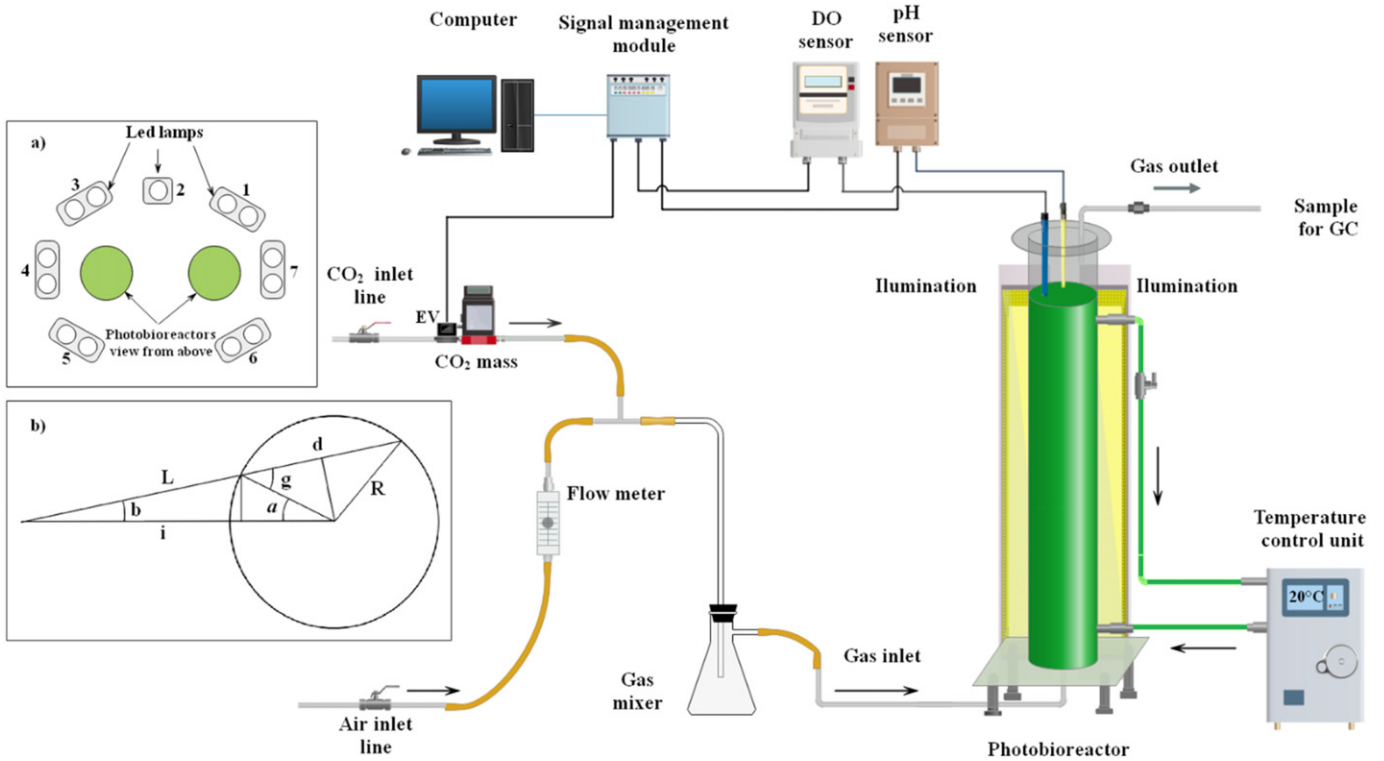
Fig. 1. Schematic of the configuration set-up. (a) light distribution (b) trigonometric relationships.

controlled and monitored using LabVIEW™ 2015 (v.15.0f2, National Instruments™, USA) with cDAQ Chassis (NO-9184) and modules for analog input (NI-9208) and a digital input–output interface (NI-9375). Combo medium [14] enriched in phosphorus (5 mM) and nitrogen (2.5 mM $NaNO_3$ and 2.5 mM NH_4Cl) was used in the study and the initial biomass concentration was 80 mg TSS L^{-1}.

2.3. Analytical methods

Biomass concentration was measured as optical density at 680 nm (UV/VIS Spectroquant Pharo 300, Merck Group, Germany). A calibration curve was created to convert the optical density to biomass as dry weight (Fig. S1). 'Total Suspended Solid (TSS) dried' was determined according to the Standard Method 2540-C [15]. Nitrate and ammonium concentrations were determined using ion chromatography (Metrohm 930 Compact IC Flex, Switzerland). Gas samples were collected in Tedlar® bags (1 L, 232–01, SKC, USA) connected to the off-gas bioreactor. The CO_2 concentration was measured every 24 h by gas chromatography (450-GC, Bruker, Spain) with a Thermal Conductivity Detector.

2.4. Model development

The model describes the dynamics of carbon inorganic species, nitrogen species and biomass in the photobioreactor. The conceptualized model used is shown in Fig. 2, with the assimilation and growth kinetics expressed as a function of multiple factors, including DIC inhibition and NH_4^+ inhibition of NO_3^- assimilation.

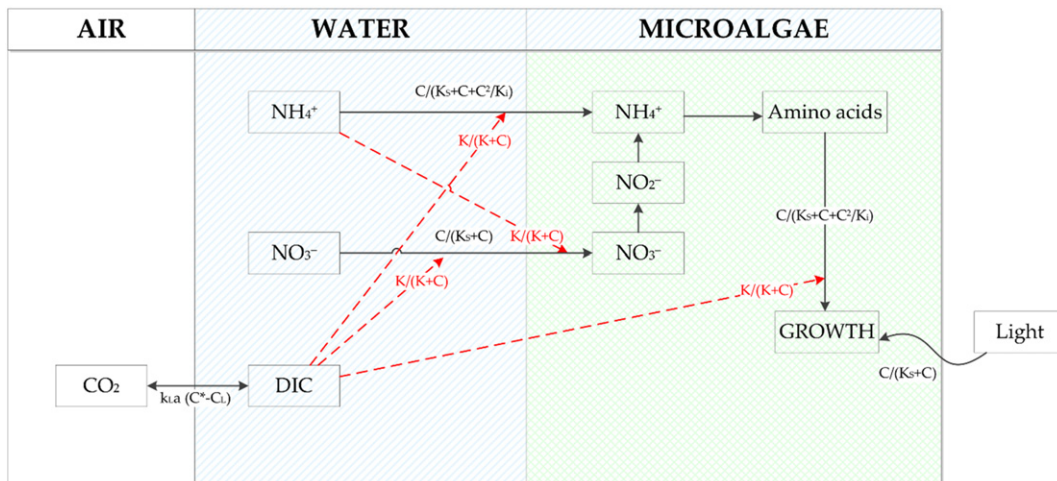The model presented herein includes the following assumptions:

Fig. 2. Schematic diagram of model conceptualization for ammonium, nitrate and carbon dioxide uptake.

– The column is considered as a completely mixed batch reactor. This assumption is made due to the low biological reaction rate versus the mixing caused by bubbles [16].
– The oxygen concentration remains constant and is in equilibrium with the gas phase.
– The oxygen concentration is below inhibitory levels.
– The DIC concentration was equal to the sum of H_2CO_3, HCO_3^- and CO_3^{2-}, being all the compounds in equilibrium with CO_2 in the gas phase.
– The biomass-nitrogen yield can be obtained from the initial nitrogen concentration and pH.
– NO_3^- is transported into the cell, where it is transformed into NO_2^- and then NH_4^+, with the conversion into NO_2^- and NH_4^+ being much faster than NO_3^- absorption (Fig. 2) [17,18].
– NO_3^- absorption rate can be expressed with a Monod-type equation and it is inhibited by NH_4^+ concentration.
– NH_4^+ absorption rate can be expressed with a Haldane-type equation.
– NH_4^+ is incorporated as amino acids and the assimilation rate of nitrogen is much faster than the specific growth rate.
– The specific growth rate can be expressed with a Haldane-type equation.
– NO_3^- absorption rate, NH_4^+ absorption rate and specific growth rate are inhibited by DIC.
– The effect of light intensity can be expressed with a Monod-type equation.

2.4.1. Growth kinetics, rate equations and mass balances

The specific growth rate (μ) was described by a pseudo-triple substrate expression [Equation 1]. The growth rate was considered to be a function of assimilated nitrogen concentration, DIC concentration and light intensity. In the case of nitrogen, the factors considered were nutrient limitation and inhibition by the Haldane model. Inhibition was considered for DIC and the Monod model was used for light intensity consumption.

$$\mu = \mu_{\max} \frac{C_N}{K_{s,N} + C_N + {(C_N)^2}/{K_{i,N}}} \frac{K_{DIC,X}}{K_{DIC,X} + C_{DIC}} \frac{I_{ave}}{K_{s,I} + I_{ave}} \qquad \text{[Equation 1]}$$

The specific nitrate consumption ($q_{s,NO3}$) was also described by a pseudo-triple substrate expression using [Equation 2]. The factors considered were functions of nitrate, ammonium and carbon DIC concentrations. For nitrate the Monod model was used, whereas inhibition was considered for ammonium and DIC uptake.

$$q_{s,NO3} = q_{\max,NO3} \frac{C_{L,NO3}}{K_{s,NO3} + C_{L,NO3}} \frac{K_{NH4}}{K_{NH4} + C_{L,NH4}} \frac{K_{DIC,NO3}}{K_{DIC,NO3} + C_{DIC}} \qquad \text{[Equation 2]}$$

The specific ammonium consumption ($q_{s,NH4}$) can be expressed in terms of ammonium concentration (Haldane model) and DIC concentration (inhibition model) according to Equation 3.

$$q_{s,NH4} = q_{\max,NH4} \frac{C_{L,NH4}}{K_{s,NH4} + C_{L,NH4} + {(C_{L,NH4})^2}/{K_{i,NH4}}} \frac{K_{DIC,NH4}}{K_{DIC,NH4} + C_{DIC}} \qquad \text{[Equation 3]}$$

The dynamic model considered the CO_2 mass transfer from the gas phase to the liquid phase and the CO_2, nitrate, ammonium and assimilated nitrogen uptakes. The mass balance of the CO_2 from the gas to the liquid phase can be written as:

$$\frac{dC_{G,CO2}}{dt} = \frac{F_G}{V_G}\left(C_{G,CO2,IN} - C_{G,CO2}\right) - \frac{V_L}{V_G} \cdot k_L a \cdot \left(C_{L,CO2}^* - C_{L,CO2}\right) \quad \text{[Equation 4]}$$

According to Henry's Law [Equation 5] and on the assumption that the DIC concentration was equal to the $C^*_{L,CO2}$ [Equation 6], $C^*_{L,CO2}$ can be obtained by [Equation 7]. Where 'm' can be obtained from [Equation 8] as a function of the pH, Henry's constant and dissociation constants [19].

$$H_{CO2} = \frac{C_{G,CO2}}{C_{L,CO2}^*} \qquad \text{[Equation 5]}$$

$$C_{DIC} = C_{L,CO2}^* = C_{L,H_2CO_3} + C_{L,HCO_3^-} + C_{L,CO_3^{2-}} \qquad \text{[Equation 6]}$$

$$C_{L,CO2}^* = \frac{C_{G,CO2}}{m} \qquad \text{[Equation 7]}$$

$$m = \frac{H_{CO2}}{1 + \dfrac{k_{a,1}}{10^{-pH}} + \dfrac{k_{a,1}k_{a,2}}{10^{-2 \cdot pH}}} \qquad \text{[Equation 8]}$$

The mass balance for CO_2 in the liquid phase, nitrate, ammonium and nitrogen assimilated can be written as follows:

$$\frac{dC_{L,CO2}}{dt} = k_L a \cdot \left(C_{L,CO2}^* - C_{L,CO2}\right) - \frac{\mu}{Y_{x/CO2}} \cdot X \qquad \text{[Equation 9]}$$

$$\frac{dC_{L,NO3}}{dt} = -q_{S,NO3} \cdot X \qquad \text{[Equation 10]}$$

$$\frac{dC_{L,NH4}}{dt} = (q_{S,NO3} - q_{S,NH4}) \cdot X \qquad \text{[Equation 11]}$$

$$\frac{dC_N}{dt} = -\frac{\mu}{Y_{x/N}} \cdot X \qquad \text{[Equation 12]}$$

$$\frac{dX}{dt} = \mu \cdot X \qquad \text{[Equation 13]}$$

The yield coefficient for the biomass produced by nitrogen consumed ($Y_{X/N}$) was determined using the results in this study plus those of ten independent experiments (unpublished data). For each such experiment, the total biomass growth divided by the total nitrogen consumed was obtained with [Equation 14].

$$Y_{x/N} = \frac{\Delta X}{-\Delta N} \qquad \text{[Equation 14]}$$

The yield coefficient was observed to be dependent on two independent variables, pH and initial nitrogen concentration (nitrate plus ammonium). Therefore, in the simulation a second-order polynomial equation [20] was used to obtain an empirical prediction of the yield coefficient [Equation 15].

$$Y = a_o + a_1 \cdot X_1 + a_2 \cdot X_2 + a_{11} \cdot (X_1)^2 + a_{22} \cdot (X_2)^2 + a_{12} \cdot X_1 \cdot X_2 \qquad \text{[Equation 15]}$$

where Y is the predicted response (yield coefficient); a_0 is the intercept; a_1 and a_2 are the linear coefficients; a_{11} and a_{22} are the squared coefficients; a_{12} is an interaction coefficient; X_1 and X_2 are the coded independent factors, namely pH and the initial nitrogen concentration, respectively. Statgraphics Centurion 18 (v18.1.02, Statgraphics Technologies, Inc.) was used to carry out the regression analysis on the experimental data.

Biomass productivity was obtained with [Equation 16] [21], where X_{max} is the maximum microalgae concentration, X_0 is the initial

microalgae concentration and t_m and t_0 are the times required to reach X_{max} and X_0, respectively.

$$P_B = \frac{\Delta X}{\Delta t} = \frac{(X_{max} - X_0)}{(t_m - t_0)} \qquad \text{[Equation 16]}$$

2.4.2. Photon flux density

The photon flux density (PFD) was measured as active photosynthetic radiation in the wavelength range between 400 and 700 nm. The incident PFD (PFD_{IN}) was measured on the surface of the photobioreactor at the minimum distance between the reactor and the light source using an SQ-420 smart Quantum Sensor (Apogee Instruments, Inc.). In the average PFD (PFD_{AVE}) calculations it was assumed that reactor B completely eclipses focus 4 on reactor A and reactor A completely eclipses focus 7 on reactor B (Fig. 1a).

PFD_{AVE} and the light gradients inside the photobioreactors were calculated using Beer's Law [Equation 17].

$$PFD_{AVE} = PFD_{IN} \cdot e^{-a_X \cdot X \cdot \delta} \qquad \text{[Equation 17]}$$

$$a_X = \sum_{400}^{700} a_X(\lambda) \qquad \text{[Equation 18]}$$

where a_X is the specific absorption coefficient of the biomass, X is the biomass concentration and δ is the light path inside the reactor. Coefficient a_X was calculated by measuring the absorbance between 400 and 700 nm with different biomass concentrations and it was weighted considering the relative intensity of the lamp [Equation 18] [22].

PFD_{IN} was also estimated with Beer's Law as follows.

$$PFD_{IN} = PFD_0 \cdot e^{-a_a \cdot L \cdot A_m} \qquad \text{[Equation 19]}$$

where PFD_0 was measured at the light source surface, a_a is the air absorption coefficient, L is the length between the light focus and photobioreactor surface and A_m is the methacrylate absorbance.

PFD_{AVE} inside the photobioreactor was determined by the numerical integration of [Equation 17] between $\beta = -\beta_{max}$ and $\beta = \beta_{max}$; and $\delta = 0$ and $\delta = 2R$.

$$PFD_{AVE} = \frac{\iint_{low}^{high} PFD_{IN}(\beta) \cdot e^{-a_X \cdot X \cdot \delta(\beta,\delta)} \cdot d\delta \cdot d\beta}{\iint_{low}^{high} 1 \cdot d\delta \cdot d\beta} \qquad \text{[Equation 20]}$$

The trigonometric relationships considered are shown in Fig. 1b.

Table 1
Parameters used in the calibration stage.

Parameter	Value	Reference
V_G	$4.24 \cdot 10^{-5}$ m^3	Experimental
V_L	$8 \cdot 10^{-3}$ m^3	Experimental
F_G	$4.8 \cdot 10^{-2}$ m^3 h^{-1}	Experimental
$K_La_{,O2}$	26.06 h^{-1}	Experimental
K_La [1]	$K_La_{,O2} \cdot 0.9$ h^{-1}	[23]
H_{CO2}	1.01	[24]
$k_{a,1}$	$4.46 \cdot 10^{-7}$ mol L^{-1}	[19]
$k_{a,2}$	$4.67 \cdot 10^{-11}$ mol L^{-1}	[19]
$Y_{X/CO2}$	0.487 g TSS g^{-1} CO$_2$	Experimental
a_x	0.268 m^2 g^{-1}	Experimental
A_m	0.083	Experimental

[1] for CO$_2$.

2.4.3. Model calibration and validation

The calibration stage was carried out with four experiments at inlet CO_2 concentrations of 5, 10, 20 and 30% (operational conditions detailed in Section 2.2). Ammonium, nitrate and biomass concentrations were measured throughout the experiment (408 h). The parameters used in the calibration are listed in Table 1 [23,24]. The oxygen mass transfer coefficient (K_La) was measured by the dynamic 'gas out-gas in' method. The biomass-carbon dioxide yield ($Y_{X/CO2}$) was obtained by a total carbon content determination by elementary analysis (Leco® CHNS 932, Leco Corporation, USA) using the Dumas combustion method.

The developed model was calibrated with biological kinetic parameters. The solution was obtained using MATLAB® R2019a (The MathWorks Inc., USA). The objective functions to minimize for each simulated period were:

$$OF_{NH4} = \sum_{j=1}^{M} \sqrt{\sum_{i=1}^{N} \left[C_{L,NO3} \left(q_{max,NH4}, K_{S,NH4}, K_{i,NH4}, K_{DIC,NH4} \right) - C_{L,NH4}^{exp} \right]^2}$$

$$\text{[Equation 21]}$$

$$OF_{NO3} = \sum_{j=1}^{M} \sqrt{\sum_{i=1}^{N} \left[C_{L,NO3} \left(q_{max,NO3}, K_{S,NO3}, K_{NH4}, K_{DIC,NO3} \right) - C_{L,NO3}^{exp} \right]^2}$$

$$\text{[Equation 22]}$$

$$OF_x = \sum_{j=1}^{M} \sqrt{\sum_{i=1}^{N} \left[X \left(\mu_{max}, K_{S,N}, K_{i,N}, K_{DIC,X}, K_{S,I} \right) - X^{exp} \right]^2} \qquad \text{[Equation 23]}$$

The validation experiment was designed by considering two phases, namely (i) a batch operation (312 h) with an initial nitrate concentration of 2 mM NO_3^- followed by (ii) continuous operation (312 h to 600 h) with a liquid flow rate of 1.55 L d^{-1} and an inlet ammonium concentration of 3.4 $\pm$ 0.34 mM NH_4^+. The ammonium source was landfill leachate, which is the same as that used in the consortium isolation (Section 2.1). The inlet CO_2 concentration was 2.5%, the initial pH was 6.67 and the temperature was 21.0 $\pm$ 0.7°C.

A sensitivity analysis was carried out on the effect of small variations in the kinetic parameters on biomass, nitrate and ammonium concentrations. The model was run (500 runs) with random values of parameters bounded within 99.5 and 100.5% of the initial kinetic parameter value. A plot of response versus the parameter allows the sensitivity to be evaluated.

3. Results and discussion

3.1. Isolation

A nonaxenic consortium was obtained after three cycles. The microalgae had a homogenous size and they were spherical, with an average size of 3.67 $\pm$ 0.6 μm (Fig. S2). This consortium has previously been used to study a chemical-enzymatic method to obtain protein and amino acids [25]. Callejo-López et al. [25] found that the consortium was a resistant microalgae with a total protein content of 39.5%. Moreover, the consortium was able to store lipids under nitrogen and phosphorus limitation up to 53% after 9 d with Combo medium at 2 mM (NaNO$_3$) (data not published).

In order to know the consortium composition, a genetic analysis should be performed because the morphological determination led to various constraints in performing the classification procedure [26]. However, the predominant species, based on the above data (size, protein and lipid concentration), could belong to *Nannochloropsis* sp. The size is in the range measured by other authors. For instance, Baroni et al. [27] studied the effect of nitrogen depletion on the shape and cellular size of *Nannochloropsis salina*, with a measured size of 3–4

μm. Kandilian et al. [28], in an analysis of the properties of cells at different irradiances, found a cell size of 2.52–2.63 μm for *N. oculata*. Moreover, the protein content is similar to that found by Safi et al. [14] of 46.5% protein extract for *N. salina* and lipid accumulations of 36.5 and 60.4% were found for *N. salina* and *Nannochloropsis granulata*, respectively [29]. Nevertheless, *Chlorella sorokiniana* also has a small size, between 2–4.5 μm [30] and can accumulate lipids (from 28% to 43%) although it has a lower tolerance to high CO_2 concentrations [31,32]. So, further studies should be conducted to properly determine the consortium composition.

3.2. Model calibration

The maximum biomass concentration achieved in this study was 1.8 g L^{-1} (Fig. 3a) at the lowest inlet CO_2 concentration (5%). As can be seen from Fig. 3a, an increase in the inlet concentration had a negative effect on the maximum biomass concentration and on the biomass productivity (Table 2). Experimental values were adjusted by the

Table 2
Experimental growth parameters at different inlet CO_2 concentrations.

% CO_2	X_{max} (g TSS L^{-1})	P_B[a] (g TSS L^{-1}d^{-1})
5	1.80	0.101
10	1.68	0.090
20	1.30	0.065
30	0.69	0.038

[a] Obtained by [Equation 16].

model with error values of less than 5% — except for inlet concentrations of 5 and 30% (Fig. 3b).

In relation to previous studies on the effect of CO_2, similar values were found by Razzak et al. [33], with the highest productivity being 0.088 g TSS L^{-1} d^{-1} for *N. oculata* under mixotrophic conditions at 8% CO_2 in a bubble column photobioreactor for the treatment of wastewater. Similar productivities (0.08 g TSS L^{-1} d^{-1}) were found by Kumar et al. [32] using flue gas at 100% (15.65% CO_2) in an airlift
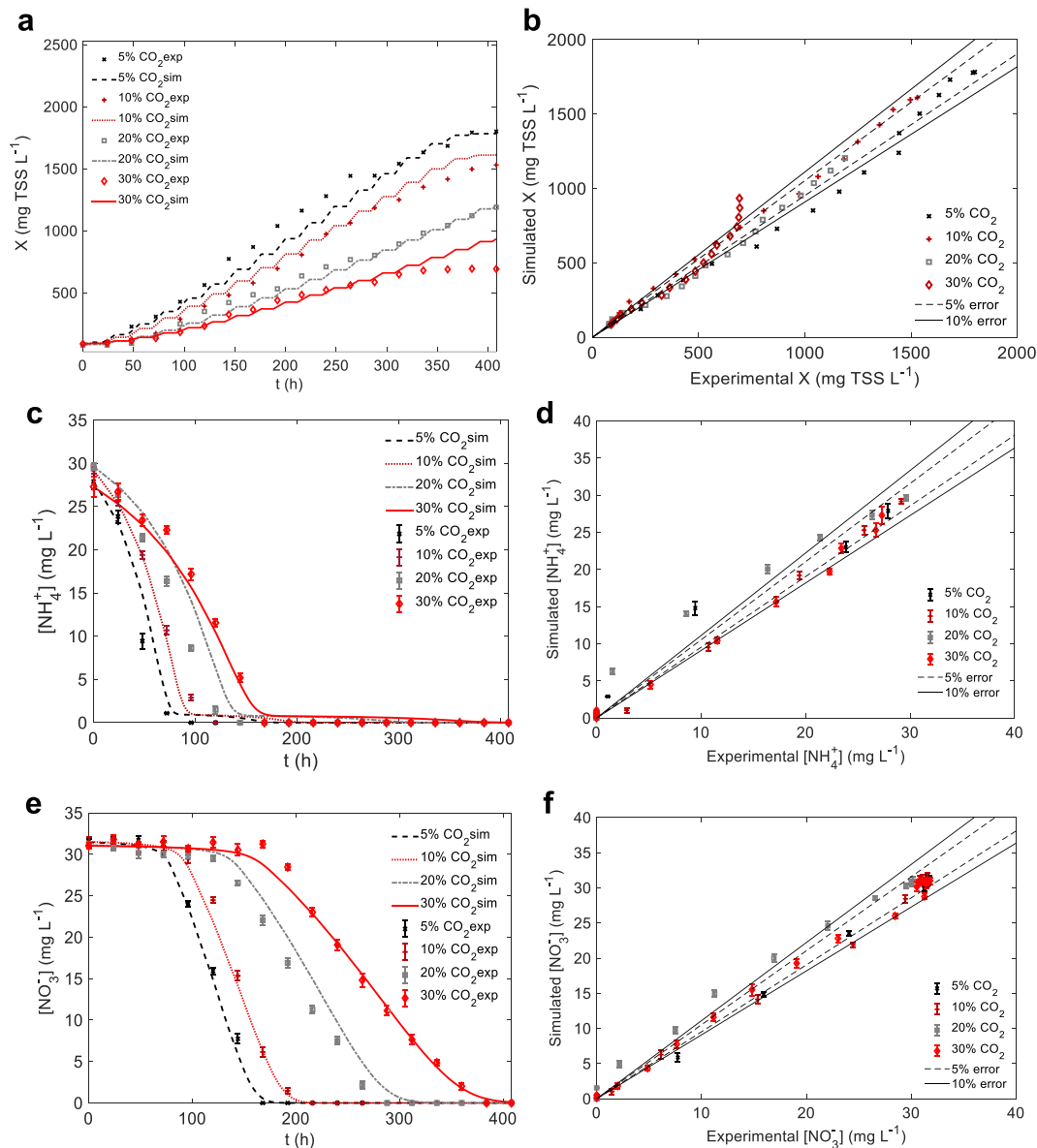

Fig. 3. Model calibration. Experimental and simulated values: (a) biomass concentration; (b) error for biomass concentration; (c) ammonium concentration; (d) error for ammonium concentration; (e) nitrate concentration; (f) error for nitrate concentration.
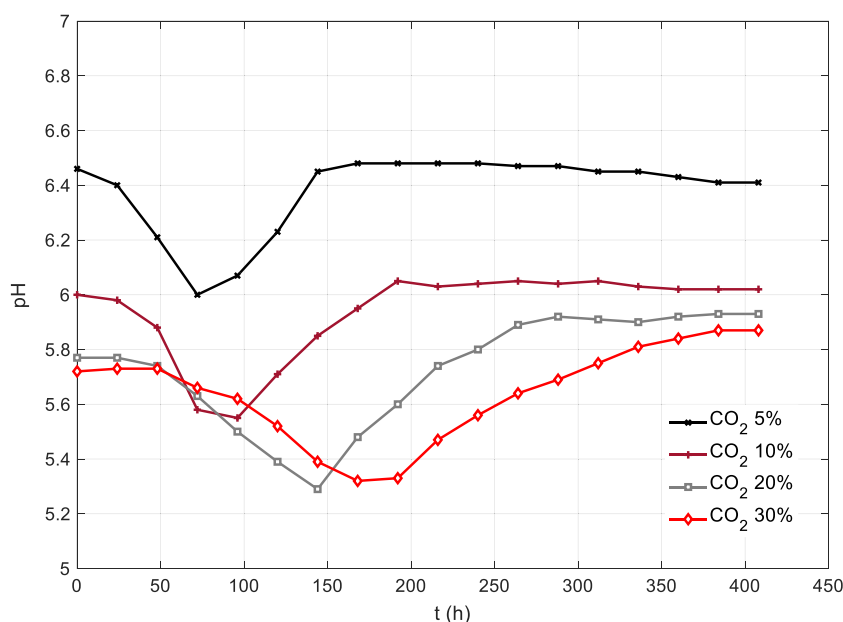
Fig. 4. Profiles of pH in the model calibration experiment.

reactor with *C. sorokiniana*. Nevertheless, Razzak et al. [33] for *N. oculata* found a decrease in the productivity to 0.077 g TSS L^{-1} d^{-1} at 12% CO_2, whereas in this study, an inlet CO_2 feed of 20% was required to achieve the same productivity. Therefore, the performance of the consortium used in this study was better. The biomass grew even at high inlet CO_2 concentrations (20 and 30%) for a prolonged operation time of 400 h. Inhibition of biomass growth could be due to the decrease in pH [3,12,34]. In this study, the biomass was successfully grown at a pH between 5.3 and 6.5 (Fig. 4), and this behavior is similar to that observed by other authors [3,35]. The consortium began to assimilate the ammonium source first and then the nitrate source (Fig. 3c and Fig. 3f). This assimilation order, produced a pH swing in the culture, the pH decreased while ammonium was in the culture. Once ammonium was assimilated, the pH began to rise due to nitrate consumption. Hence, the isolated consortium is able to grow at a high CO_2 inlet concentration and therefore it can be used for CO_2 capture from CO_2-rich gases.

Ammonium and nitrate concentrations were adjusted by the model with an error value of less than 10% for nitrate (Fig. 3f), although for ammonium some values had errors higher than 10% at inlet CO_2 concentrations of 5 and 30% (Fig. 3d).

3.3. Kinetic characterization

Nitrate must be reduced to ammonium before it is assimilated by the biomass but ammonium can be assimilated directly [17]. This behavior was included in the equation for specific nitrate consumption ($q_{s,NO3}$; [Equation 2]) with the second term for ammonium inhibition (K_{NH4+}

Table 3
Ammonia, nitrate and total nitrogen consumption rates at different inlet CO_2 concentrations.

% CO_2	N-NH_4^+ (mg $L^{-1}d^{-1}$)	N-NO_3^- (mg $L^{-1}d^{-1}$)	N total (mg $L^{-1}d^{-1}$)
5	11.38	7.81	19.29
10	10.49	7.27	17.76
20	6.43	4.88	11.31
30	5.57	3.56	9.13

= 0.75 mg N-NH_4^+ L^{-1}). It is well known that ammonium ion has a negative effect on nitrate assimilation because the nitrogen-containing species with the more reduced state (ammonium) is more readily assimilated than that with the higher oxidation state (nitrate) [17,18]. The nitrogen consumption rate was also calculated from the slope of the straight part of the curve in Fig. 3c and Fig. 3f for ammonium and nitrate, respectively (Table 3). It can be seen that CO_2 had a negative effect on the ammonium and nitrate consumption. The total nitrogen consumption was in the range 9.13–19.29 mgN L^{-1} d^{-1}, which is similar to the values obtained by Mennaa et al. [36] for *Scenedesmus obliquus* of 13.49 mgN L^{-1} d^{-1} using air without an external source of CO_2.

The second order polynomial that describes $Y_{X/N}$ is as follows [Equation 24] and Fig. 5b):

$$Y_{X/N} = -1928.41 + 555.97 \cdot pH + 6.17 \cdot N_{ini} - 38.63 \cdot pH^2 \quad \text{[Equation 24]}$$

$$-1.22 \cdot pH \cdot N_{ini} + 0.01 \cdot N_{ini}^2$$

The average pH ranged between 5.93 and 6.78 and initial Nitrogen (N_{ini}) ranged between 11.0 and 61.8 g m^{-3}. The equation predicts with a high level of similarity the experimental data. The R-squared was 99.80%, the residual standard deviation was 0.78 and the mean absolute error was 0.38. Moreover, the plot of residuals versus predicted values (Fig. 5a) does not show any linear trend and this is consistent with a good correlation between experimental and simulated data. Experimental $Y_{X/N}$ values were between 10.35 and 51.85 g TSS gN^{-1}. Similar values to that measured in this study can be found in the literature, e.g., 5.46 [37], 10.96 [38] and 15.84 g TSS gN^{-1} [39], although at high pH and low initial nitrogen our values are higher than those published previously. The $Y_{X/N}$ value is also related to the phase of the growth curve [21]. For instance, elemental analysis of the consortium used in this study gave values of 33.87 and 11.12 g TSS gN^{-1} after the exponential growth phase (7 d) and in the exponential growth phase, respectively.

The PFD_{AVE} that enters the photobioreactor was 338 ± 3 µmol m^{-2} s^{-1}, including air and methacrylate absorbance. The PFD_{AVE} was calculated as a function of biomass concentration and the values ranged between 123 µmol m^{-2} s^{-1} for the lowest concentration (78 mg TSS L^{-1}) and 9
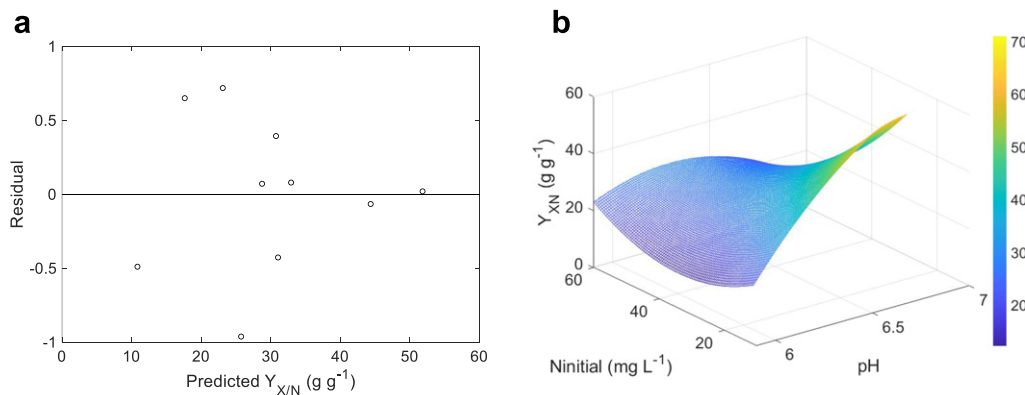
a

b

Fig. 5. (a) Residual vs predicted $Y_{X/N}$. (b) Surface plot of the predicted $Y_{X/N}$ as function of pH a $N_{initial}$.

μmol m^{-2} s^{-1} for the highest biomass concentration (1799 mg TSS L^{-1}). Therefore, the amount of light energy absorbed was in the range 215–329 μmol m^{-2} s^{-1}. Barbosa et al. [22] reported a PFD_{AVE} for a flat-plane reactor as a function of dilution rate, with values from around 110 to around 780 μmol m^{-2} s^{-1} for dilution rate values between 0.018 and 0.119 h^{-1}.

The 13 kinetic parameters obtained in the model calibration are listed in Table 4 along with comparable values from other studies [5,7,9,37–47]. Numerous mathematical models can be found in the literature [48]. However, the models developed for *Nannochloropsis* are restricted to low CO_2 concentrations, e.g., 0.34–1.34% [4], 0.5–2% [5], 0.5–4% [6], 5% [7] and 5–8% [3]. Nevertheless, Chiu et al. [34] studied a maximum CO_2 concentration of 15% using *N. oculata* for lipid production. The values of the kinetic parameters are usually different for different published studies. However, the values obtained in this work are similar to those published by Surendhiran et al. [41]. They employed a logistical model for growth kinetics and obtained maximum specific growth rates of 0.447 and 0.4053 h^{-1} for *N. oculata*

under non-limited nitrogen and nitrogen-depleted conditions, respectively. For other species of *Nannochloropsis* the maximum specific growth rate is usually lower [7,42]: 0.037 h^{-1} for *Nannochloropsis gaditana*, 0.039 h^{-1} for *N. salina*, 0.08 h^{-1} *Nannochloropsis oceanica*. Similar maximum specific growth rates have been measured for other strains, such as *Auxenochlorella protothecoides* (0.46 h^{-1}) [49].

In relation to the rest of the parameters (Table 4), the maximum specific nitrate and ammonium uptakes were similar. The highest Monod half-saturation constant was for nitrate; therefore, the order for substrate affinity was assimilated nitrogen > ammonium > nitrate, which is consistent with the model conceptualization (Fig. 2) and the results of others studies [17,18]. In relation to the inhibition constants, assimilated nitrogen had a higher value than ammonium, thus confirming the higher affinity of assimilated nitrogen vs. ammonium. It is worth noting the high value of the inhibition constant for DIC, which is probably due to the higher inlet CO_2 concentration used in this study. The model proposed in this study included inhibition of DIC in the ammonium uptake ($K_{DIC,NH4}$) and in the nitrate uptake ($K_{DIC,NO3}$) but, to our knowledge, previous models have not considered these factors, which could be due to the lower inlet CO_2 reported in other studies. Moreover, inhibition of the nitrate uptake by ammonium (K_{NH4}) was considered and, in this case, we only found one study in which inhibition was considered depending on the nitrogen concentration for the specific lipid accumulation rate [47].

3.4. Model validation

A comparison of the experimental values corresponding to the validation experiment and the simulated experiments is provided in Fig. 6a.

As can been seen, the model was able to predict the biomass concentration in the batch phase (0–312 h) and in continuous operation (312–600 h). According to [Equation 1], in periods of darkness, the model simulates the non-growth of biomass. The maximum errors found were in the batch operation, with simulated values lower than experimental ones. It is important to mention that the validation conditions differ not only in the operation mode but also in the nitrogen source. Despite the use of landfill leachate, for 70% of the experimental data the error was lower than 10% (Fig. 6b). Therefore, it can be considered that the model was suitably validated and that it will be applicable to other operating conditions. Applying the model to different scenarios could reduce costs and time spent on experimentation. It could be applied to analyze the effect of controlling pH by a buffer or an automated control, due to the close relationship between pH and DIC concentration. It will also allow its use in the simulation of the treatment of gaseous effluents with a high concentration of CO_2 such as combustion gases or biogas. Also, in the

Table 4
Kinetic parameters.

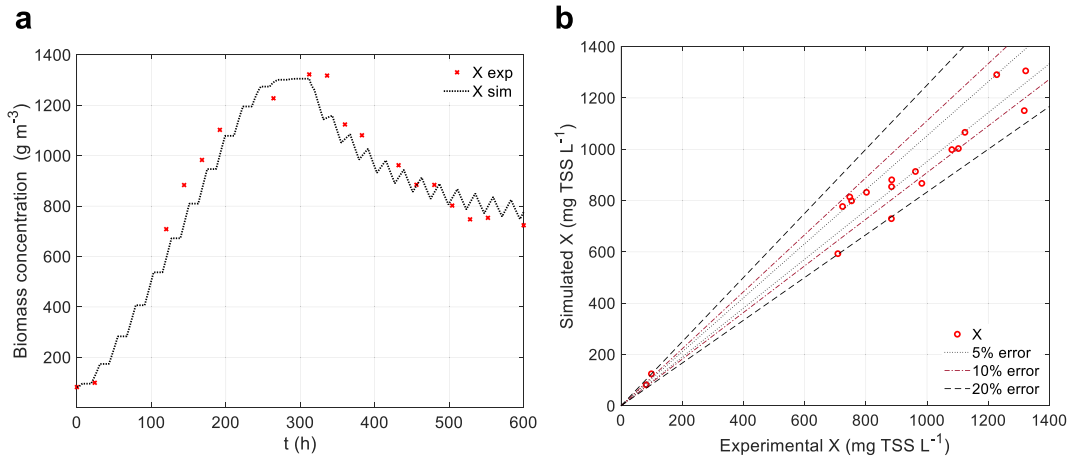| Parameter	Value	Comparable values from the literature
μ_{max} (h^{-1})	0.43	0.447 for *N. oculata* (non-limited nitrogen) [40]
		0.4053 for *N. oculata* (depleted nitrogen) [40]
		0.039 for *N. gaditana* [7]
		0.08 for *N. salina* [7]
		0.46 for *Auxenochlorella protothecoides* [41]
$q_{max,NO3}$ (mg N-NO_3^- mg TSS^{-1} h^{-1})	$9.90 \cdot 10^{-3}$	$1.67 \cdot 10^{-4}$ for *N. salina* [42]
$q_{max,NH4}$ (mg N-NH_4^+ mg TSS^{-1} h^{-1})	$6.80 \cdot 10^{-3}$	$2.5 \cdot 10^{-2}$ for *Pseudochlorococcum sp.* [43]
$K_{s,N}$ (mg N L^{-1})	1.72	1.78 for *Chlorella sp.* [9]
		0.07 for *C. vulgaris* [44]
$K_{s,NO3}$ (mg N-NO_3^- L^{-1})	11.31	0.30 for *C. vulgaris* [39]
		0.09–3.94 for *Dunaliella tertiolecta* N-NO_3^- (75–900 mgL^{-1}) [37]
$K_{s,NH4}$ (mg N-NH_4^+ L^{-1})	3.01	0.30 for *C. vulgaris* [39]
		0.01 for Algae-bacteria consortium [38]
$K_{s,I}$ (μmol m^{-2} s^{-1})	368.52	183.13 for *Nannochloropsis sp.* [45]
		200 for *N. salina* [42]
$K_{i,N}$ (mg N L^{-1})	774.18	364 for *Chlorella sp.* [9]
		625 for *Chlamydomonas reinhardtii* with organic carbon source [46]
		113 for *Chlamydomonas reinhardtii* with organic carbon source [47]
$K_{i,NH4}$ (mg N-NH_4^+ L^{-1})	39.14	0.03 for *C. vulgaris* [39]
$K_{DIC,X}$ (mg C L^{-1})	404.84	55.2 for *N. salina* (mg C-CO_2 L^{-1}) [5]
K_{NH4} (mg N-NH_4^+ L^{-1})	0.75	–
$K_{DIC,NO3}$ (mg C L^{-1})	75.77	–
$K_{DIC,NH4}$ (mg C L^{-1})	237.18	–

Fig. 6. Model validation (a) Evolution of experimental biomass vs. simulated. (b) Error of experimental biomass vs. simulated.

simulation of different control methods that minimize the inhibitory effect of high concentrations of CO_2, such as the gas supply cut-off or the alternative supply of gas and air.

The sensitivity analysis showed that the biomass was influenced by μ_{max} and $K_{s,I}$. It can be seen from Fig. 7a that μmax had a positive effect of 2606.6 (mg TSS L^{-1})/(h^{-1}) and $K_{s,I}$ had a negative effect of -2.72 (mg TSS L^{-1})/(μmol m^{-2} s^{-1}). The ammonium concentration was sensitive to $q_{max,NH4}$ and $K_{i,NH4}$ and both had a negative effect (Fig. 7b) on ammonium concentration of -2378.3 (mg N-NH_4^+ L^{-1})/(mg N-NH_4^+ mg TSS^{-1} h^{-1}) and -0.26 (mg N-NH_4^+ L^{-1})/(mg N-NH_4^+ L^{-1}). Nitrate concentration was influenced by μ_{max}, $K_{s,I}$ and $q_{max,NH4}$ (Fig. 7c)), where μ_{max} had a negative effect of -51.98 (mg N-NO_3^- L-

^{1})/(h^{-1}), $K_{s,I}$ had a positive effect of 0.048 (mg N-NO_3^- L^{-1})/(μmol m^{-2} s^{-1}) and $q_{max,NH4}$ had a negative effect of -3379.4 (mg N-NO_3^- L^{-1})/(mg N-NH_4^+ mg TSS^{-1} h^{-1}). As an example, the results of the sensitivity analysis for μ_{max} on biomass concentration are presented in Fig. 7d.

4. Conclusions

A second-order polynomial equation as a function of pH (5.93–6.78) and initial nitrogen concentration (11.0–61.8 g m^{-3}) can used to obtain the yield coefficient for biomass produced by nitrogen consumed, over the range10.35 to 51.85 g TSS gN^{-1}. The experimental results can be
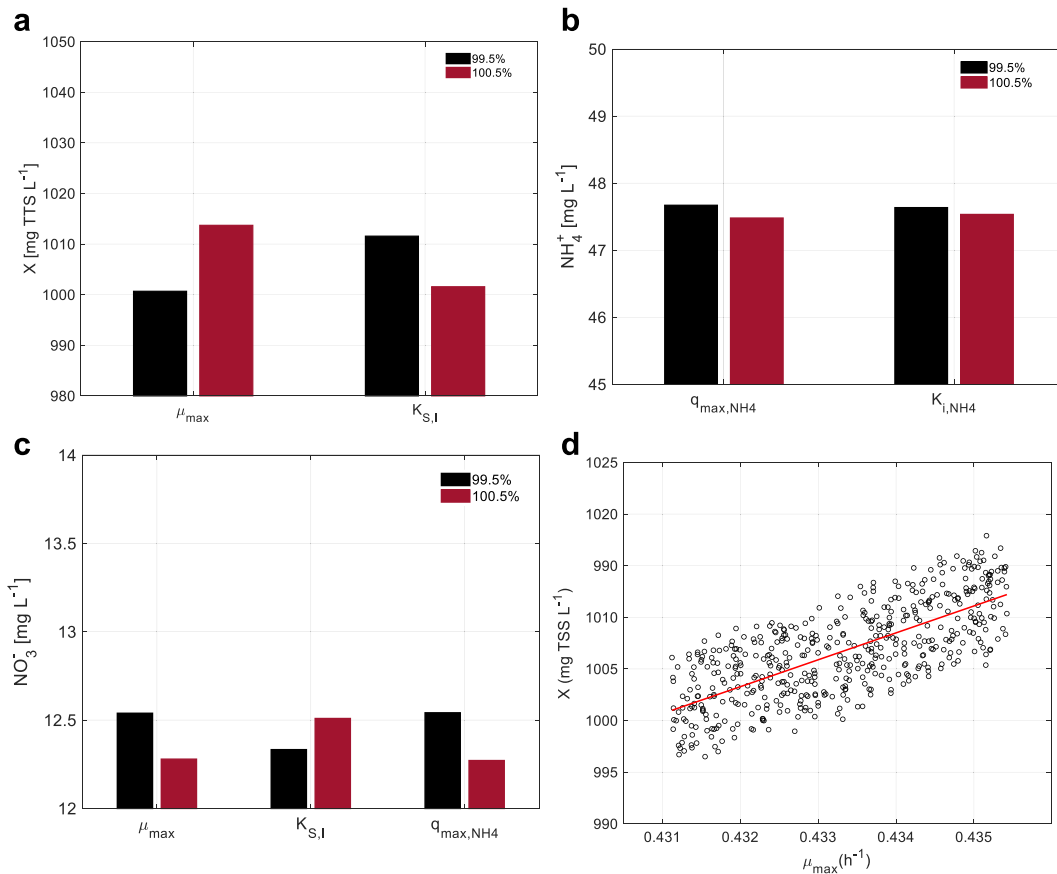

Fig. 7. Parameter sensitivity – main effects on (a) Biomass concentration (μ_{max} and $K_{s,I}$), (b) Ammonium concentration ($q_{max,NH4}$ and $K_{i,NH4}$), (c) Nitrate concentration (μ_{max}, $K_{s,I}$ and $q_{max,NH4}$) and (d) Example of analysis results (biomass concentration vs μ_{max}).

adequately predicted by the proposed mathematical model using 13 kinetic parameters with errors lower than 5% for biomass concentration (10 and 20% of CO_2) 10% for nitrate (full CO_2 range) and 10% for ammonia (10 and 20% of CO_2). In addition, validation was performed under operating conditions (continuous mode and leachate as nitrogen source) that were quite different from the calibration conditions. Therefore, the model that considers DIC inhibition in the ammonium and nitrate uptakes could successfully be used to simulate the operation of photobioreactors being fed with high CO_2 concentrations. The order for substrate affinity was assimilated nitrogen ($K_{S,N}$ 1.73 mg N L^{-1}) > ammonium ($K_{S,NH4}$ 3.01 mg N-NH_4^+ L^{-1}) > nitrate ($K_{S,NO3}$ 11.31 mg N-NO_3^- L^{-1}), which confirms the applicability of the proposed conceptual model.

Financial support

Conflict of interest

None.

Supplementary material

https://doi.org/10.1016/j.ejbt.2020.01.006

References

[1] Farrelly DJ, Everard CD, Fagan CC, et al. Carbon sequestration and the role of biological carbon mitigation: A review. Renew Sustain Energy Rev 2013;21:712–27. https://doi.org/10.1016/j.rser.2012.12.038.

[2] Ramírez M, Gómez J, Cantero D. Biogas: Sources, purification and uses. Biogas. In: Sivakumar S, Sharma UC, Prasad R, editors. Energy science and technology. Hydrogen and other technologies sources, purification and usesUSA: Studium Press LLC; 2015. p. 296–323.

[3] Hsueh HT, Li WJ, Chen HH, et al. Carbon bio-fixation by photosynthesis of *Thermosynechococcus* sp. CL-1 *and Nannochloropsis oculta*. J Photochem Photobiol B 2009;95(1):33–9. https://doi.org/10.1016/j.jphotobiol.2008.11.010. PMid: 19167907.

[4] Shene C, Chisti Y, Bustamante M, et al. Effect of CO_2 in the aeration gas on cultivation of the microalga *Nannochloropsis oculata*: Experimental study and mathematical modeling of CO_2 assimilation. Algal Res 2016;13:16–29. https://doi.org/10.1016/j.algal.2015.11.005.

[5] Pegallapati A, Nirmalakhandan N. Modeling algal growth in bubble columns under sparging with CO_2-enriched air. Bioresour Technol 2012;124:137–45. https://doi.org/10.1016/j.biortech.2012.08.026. PMid: 22989642.

[6] Muharam Y, Dianursanti, Pramadana AB, et al. Modelling and simulation of a bubble column photobioreactor for the cultivation of microalgae *Nannochloropsis salina*. Chem Eng Trans 2017;56:1555–60. https://doi.org/10.3303/CET1756260.

[7] Pfaffinger C, Schöne D, Trunz S, et al. Model-based optimization of microalgae areal productivity in flat-plate gas-lift photobioreactors. Algal Res 2016;20:153–63. https://doi.org/10.1016/j.algal.2016.10.002.

[8] Kasiri S, Ulrich A, Prasad V. Kinetic modeling and optimization of carbon dioxide fixation using microalgae cultivated in oil-sands process water. Chem Eng Sci 2015; 137:697–711. https://doi.org/10.1016/j.ces.2015.07.004.

[9] Lee E, Zhang Q. Integrated co-limitation kinetic model for microalgae growth in anaerobically digested municipal sludge centrate. Algal Res 2016;18:15–24. https://doi.org/10.1016/j.algal.2016.05.019.

[10] Kilham SS, Kreeger D, Lynn SG, et al. COMBO: A defined freshwater culture medium for algae and zooplankton. Hydrobiologia 1998;377:147–59. https://doi.org/10.1023/A:1003231628456.

[11] Andersen RA, Kawachi M. Traditional microalgae isolation techniques. In: Andersen RA, editor. Algal culturing techniques. Oxford: Elsevier Academic Press; 2005. p. 83–100. https://doi.org/10.1016/B978-012088426-1/50007-X. PMid: 15743338.

[12] Thawechai T, Cheirsilp B, Louhasakul Y, et al. Mitigation of carbon dioxide by oleaginous microalgae for lipids and pigments production: Effect of light illumination and carbon dioxide feeding strategies. Bioresour Technol 2016;219:139–49. https://doi.org/10.1016/j.biortech.2016.07.109. PMid: 27484670.

[13] Zhao B, Su Y. Process effect of microalgal-carbon dioxide fixation and biomass production: A review. Renew Sustain Energy Rev 2014;31:121–32. https://doi.org/10.1016/j.rser.2013.11.054.

[14] Safi C, Ursu A, Laroche C, et al. Aqueous extraction of proteins from microalgae: Effect of different cell disruption methods. Algal Res 2014;3:61–5. https://doi.org/10.1016/j.algal.2013.12.004.

[15] Clesceri LS, Greenberg A, Eaton A. Standard methods for the examination of water and waste water. . 20th edWashington, DC: American Public Health Association, American Water Works Association, Water Environment Federation; 1999; 1120 ISBN: 0875532357.

[16] McClure DD, Aboudha N, Kavanagh JM, et al. Mixing in bubble column reactors: Experimental study and CFD modeling. Chem Eng J 2015;264:291–301. https://doi.org/10.1016/j.cej.2014.11.090.

[17] Flynn KJ, Fasham MJ, Hipkin CR. Modelling the interactions between ammonium and nitrate uptake in marine phytoplankton. Philos Trans R Soc London Ser B 1997;352(1361):1625–45. https://doi.org/10.1098/rstb.1997.0145. PMC: 169207829.

[18] Sanz-Luque E, Chamizo-Ampudia A, Llamas A, et al. Understanding nitrate assimilation and its regulation in microalgae. Front Plant Sci 2015;6(899). https://doi.org/10.3389/fpls.2015.00899. PMid: 26579149.

[19] Franco-Morgado M, Alcántara C, Noyola A, et al. A study of photosynthetic biogas upgrading based on a high rate algal pond under alkaline conditions: Influence of the illumination regime. Sci Total Environ 2017;592:419–25. https://doi.org/10.1016/j.scitotenv.2017.03.077. PMid: 28340452.

[20] Montgomery DC. Design and analysis of experiments. . 5th edNew York: John Wiley & Sons, Inc.; 1997; 684 ISBN: 0471316490.

[21] Arbib Z, Ruiz J, Alvarez-Diaz P, et al. Photobiotreatment: influence of nitrogen and phosphorus ratio in wastewater on growth kinetics of *Scenedesmus obliquus*. Int J Phytoremediation 2013;15(8):774–88. https://doi.org/10.1080/15226514.2012.735291. PMid: 23819274.

[22] Barbosa MJ, Zijffers J, Nisworo A, et al. Optimization of biomass, vitamins, and carotenoid yield on light energy in a flat-panel reactor using the A-stat technique. Biotechnol Bioeng 2004;89(2):233–42. https://doi.org/10.1002/bit.20346. PMid: 15593095.

[23] Babcock R, Malda J, Radway J. Hydrodynamics and mass transfer in a tubular airlift photobioreactor. J Appl Phycol 2002;14:169–84. https://doi.org/10.1023/A:1019924226457.

[24] Sander R. Compilation of Henry's law constants (version 4.0) for water as solvent. Atmos Chem Phys 2015;15:4399–981. https://doi.org/10.5194/acp-15-4399-2015.

[25] Callejo-López J, Ramírez M, Bolívar J, et al. Main variables affecting a chemical-enzymatic method to obtain protein and amino acids from resistant microalgae. J Chem N Y 2019;2019:1390463. https://doi.org/10.1155/2019/1390463.

[26] Andersen RA, Brett RW, Potter D, et al. Phylogeny of the Eustigmatophyceae based upon 18S rDNA, with emphasis on *Nannochloropsis*. Protist 1998;149(1):61–74. https://doi.org/10.1016/S1434-4610(98)70010-0.

[27] Baroni É, Yap K, Webley PA, et al. The effect of nitrogen depletion on the cell size, shape, density and gravitational settling of *Nannochloropsis salina*, *Chlorella* sp. (marine) and *Haematococcus pluvialis*. Algal Res 2019;39:101454. https://doi.org/10.1016/j.algal.2019.101454.

[28] Kandilian R, Lee E, Pilon L. Radiation and optical properties of *Nannochloropsis oculata* grown under different irradiances and spectra. Bioresour Technol 2013; 137:63–73. https://doi.org/10.1016/j.biortech.2013.03.058. PMid: 23587810.

[29] Ma Y, Wang Z, Yu C, et al. Evaluation of the potential of 9 *Nannochloropsis* strains for biodiesel production. Bioresour Technol 2014;167:503–9. https://doi.org/10.1016/j.biortech.2014.06.047. PMid: 25013933.

[30] Lizzul A, Lekuona-Amundarain A, Purton S, et al. Characterization of *Chlorella sorokiniana*, UTEX 1230. Biology 2018;7(2):25. https://doi.org/10.3390/biology7020025. PMid: 29652809.

[31] Xia J, Gong S, Jin X, et al. Effects of simulated flue gases on growth and lipid production of *Chlorella sorokiniana* CS-01. J Cent South Univ 2013;20(3):730–6. https://doi.org/10.1007/s11771-013-1541-8.

[32] Kumar K, Banerjee D, Das D. Carbon dioxide sequestration from industrial flue gas by *Chlorella sorokiniana*. Bioresour Technol 2014;152:225–33. https://doi.org/10.1016/j.biortech.2013.10.098. PMid: 24292202.

[33] Razzak SA, Ilyas M, Ali SM, et al. Effects of CO_2 concentration and pH on mixotrophic growth of *Nannochloropsis oculata*. Appl Biochem Biotechnol 2015;176(5): 1290–302. https://doi.org/10.1007/s12010-015-1646-7. PMid: 25926014.

[34] Chiu S-Y, Kao C-Y, Tsai M-T, et al. Lipid accumulation and CO_2 utilization of *Nannochloropsis oculata* in response to CO_2 aeration. Bioresour Technol 2009;100 (2):833–8. https://doi.org/10.1016/j.biortech.2008.06.061. PMid: 18722767.

[35] Scherholz ML, Curtis WR. Achieving pH control in microalgal cultures through fed-batch addition of stoichiometrically-balanced growth media. BMC Biotechnol 2013;13:39. https://doi.org/10.1186/1472-6750-13-39. PMid: 23651806.

[36] Mennaa F, Arbib Z, Perales J. Urban wastewater treatment by seven species of microalgae and an algal bloom: Biomass production, N and P removal kinetics and harvestability. Water Res 2015;83:42–51. https://doi.org/10.1016/j.watres.2015.06.007. PMid: 26117372.

[37] Fré N, das Chagas A, Rech R, et al. Kinetic modeling of *Dunaliella tertiolecta* growth under different nitrogen concentrations. Chem Eng Technol 2016;39(9):1716–22. https://doi.org/10.1002/ceat.201500585.

[38] Yang A. Modeling and evaluation of CO_2 supply and utilization in algal ponds. Ind Eng Chem Res 2011;50(19):11181–92. https://doi.org/10.1021/ie200723w.

[39] Decostere B, Craene J, Hoey S, et al. Validation of a microalgal growth model accounting with inorganic carbon and nutrient kinetics for wastewater treatment. Chem Eng J 2016;285:189–97. https://doi.org/10.1016/j.cej.2015.09.111.

[40] Surendhiran D, Vijay M, Sivaprakash B, et al. Kinetic modeling of microalgal growth and lipid synthesis for biodiesel production. 3 Biotech 2015;5:663–9. https://doi.org/10.1007/s13205-014-0264-3. PMid: 28324516.

[41] Bernard O, Rémond B. Validation of a simple model accounting for light and temperature effect on microalgal growth. Bioresour Technol 2012;123:520–7. https://doi.org/10.1016/j.biortech.2012.07.022. PMid: 22940363.

[42] Ketheesan B, Nirmalakhandan N. Modeling microalgal growth in an airlift-driven raceway reactor. Bioresour Technol 2013;136:689–96. https://doi.org/10.1016/j.biortech.2013.02.028. PMid: 23603218.

[43] Packer A, Li Y, Andersen T, et al. Growth and neutral lipid synthesis in green microalgae: A mathematical model. Bioresour Technol 2011;102(1):111–7. https://doi.org/10.1016/j.biortech.2010.06.029. PMid: 20619638.

[44] Kim J, Liu Z, Lee J-Y, et al. Removal of nitrogen and phosphorus from municipal wastewater effluent using *Chlorella vulgaris* and its growth kinetics. Desalin Water Treat 2013;51(40–42):7800–6. https://doi.org/10.1080/19443994.2013.779938.

[45] Banerjee S, Ramaswamy S. Dynamic process model and economic analysis of microalgae cultivation in open raceway ponds. Algal Res 2017;26:330–40. https://doi.org/10.1016/j.algal.2017.08.011.

[46] Figueroa-Torres GM, Pittman JK, Theodoropoulos C. Kinetic modelling of starch and lipid formation during mixotrophic, nutrient-limited microalgal growth. Bioresour Technol 2017;241:868–78. https://doi.org/10.1016/j.biortech.2017.05.177. PMid: 28628990.

[47] Bekirogullari M, Fragkopoulos IS, Pittman JK, et al. Production of lipid-based fuels and chemicals from microalgae: An integrated experimental and model-based optimization study. Algal Res 2017;23:78–87. https://doi.org/10.1016/j.algal.2016.12.015.

[48] Darvehei P, Bahri PA, Moheimani NR. Model development for the growth of microalgae: A review. Renew Sustain Energy Rev 2018;97:233–58. https://doi.org/10.1016/j.rser.2018.08.027.

[49] la Siegler DH, McCaffrey WC, Burrell RE, et al. Optimization of microalgal productivity using an adaptive, non-linear model based strategy. Bioresour Technol 2012;104:537–46. https://doi.org/10.1016/j.biortech.2011.10.029. PMid: 22119433.